Eur. Phys. J. Special Topics **225**, 29–39 (2016)

DOI: 10.1140/epjst/e2016-02614-y

THE EUROPEAN PHYSICAL JOURNAL SPECIAL TOPICS

Regular Article

Network response synchronization enhanced by synaptic plasticity

S. Lobov[a], A. Simonov[b], I. Kastalskiy, and V. Kazantsev

Lobachevsky State University of Nizhny Novgorod, Nizhny Novgorod, Russia

Received 1 October 2015 / Received in final form 11 January 2016
Published online 29 February 2016

Abstract. Synchronization of neural network response on spatially localized periodic stimulation was studied. The network consisted of synaptically coupled spiking neurons with spike-timing-dependent synaptic plasticity (STDP). Network connectivity was defined by time evolving matrix of synaptic weights. We found that the steady-state spatial pattern of the weights could be rearranged due to locally applied external periodic stimulation. A method for visualization of synaptic weights as vector field was introduced to monitor the evolving connectivity matrix. We demonstrated that changes in the vector field and associated weight rearrangements underlay an enhancement of synchronization range.

1 Introduction

Synchronization in neuron networks is known to play an important role in brain information processing. Particularly, it underlies formation of brain rhythms contributing to encoding memory traces, planning motor tasks, performing navigation in space and other cognitive functions [1–4]. Also abnormal synchrony is associated with pathological processes [5]. At the level of single cells the synchrony between a pair or a small group of neurons may reflect the formation of functionally connected ensembles. This involves structural changes in connections between the neurons, also known as synaptic plasticity.

Synaptic plasticity is believed to be the key cellular mechanism of learning and memory in the brain. Experimental discovery of spike-timing dependent synaptic plasticity (STDP) [6,7] has sparked growing interest from the computational neuroscience field. A plethora of models explaining various experimental results and bridging the gap between neuronal and synaptic dynamics, plasticity and information processing have been proposed [8–14]. Network-level modelling has explained how local STDP rule can drive population dynamics [15,16].

However, little is known about the interplay between synaptic plasticity and synchronization. Recent computational studies were focused on local dynamics of a pair of neurons [17,18]. Sparse network-level models were mostly purposed to reveal the

[a] e-mail: losa99@yandex.ru
[b] e-mail: simonov@neuro.nnov.ru

role of STDP in synchronization in autonomous network dynamics or to provide theoretical approach to desynchronization of the network activity by external stimuli [19] or in the autonomous mode [20].

In this paper we investigate the role of synaptic plasticity in synchronization of evoked spiking neural network responses on locally applied periodic stimulation. The mechanisms of such evoked synchronization can provide understanding of information processing in living neural networks. Our network model simulates the dynamics of dissociated neural networks cultured on microelectrode arrays (MEAs) [21–24]. Experimental results have demonstrated that cultured neural networks can generate a variety of spiking patterns with highly precise timings [25,26]. It is believed that cultured networks can implement simple forms of memory [27–29]. In the experiments the network was locally stimulated by electrical pulses, and the network response was monitored. When the response became phase-locked with the stimulus and satisfied a predefined condition (e.g. spike appearance in the certain time interval or increasing average response activity) the stimulation was switched off providing the reinforcement. Such training could be associated with formation of novel synaptic pathways in the cultured network providing the required characteristics of the response. In our model we demonstrate how network responds to the local stimulation and can be adaptively synchronized by local periodic stimulation. We show how the network rearranges the synaptic weight matrix to enhance synchronization. This rearrangement is associated with STDP update rule.

2 Methods

2.1 Model

We took Izhikevich neuron [30] as a single neuron model, since being computationally efficient, it was able to reproduce spiking dynamics of most of the known neuron types. The model is described by the following equations:

$$\begin{aligned} \frac{dV_i}{dt} &= 0.04V_i^2 + 5V_i + 140 - u_i + \sqrt{2D}\xi_i + I_i; \\ \frac{du_i}{dt} &= a(bV_i - u_i); \end{aligned} \tag{1}$$

$$\text{if} \quad V_i \geq 30 \quad \text{mV}, \quad \text{then} \quad V_i \leftarrow c, \quad u_i \leftarrow u_i + d.$$

Here V represents the membrane potential of the neuron and u represents a membrane recovery variable. After the membrane potential reaches its peak ($V_{peak} = 30$ mV), the membrane voltage and the recovery variable are reset according to the equations and the neuron generates a spike transmitted to all its targets of the network. For all the neurons in the network we use parameter values corresponding to the regular spiking neuron [30]: $a = 0.02$, $b = 0.2$, $c = -65$, $d = 8$. Each neuron was exposed by a mutually independent and uncorrelated Gaussian white noise with variance D, $< \xi_i(t) >= 0$, $< \xi_i(t)\xi_j(t') >= \delta_{ij}\delta(t - t')$. We took $D = 3.2$ leading the neurons to fire with rate approximately 0.015 Hz.

Synaptic current I_i was calculated as the weighted sum of all synaptic inputs of the ith neuron:

$$I_i = \sum_j I_{max} w_{ij} y_{ij}(t); \tag{2}$$

where $I_{max} = 20$ is the maximal synaptic current, the range of index j is defined for each ith neuron by a connectivity rule described below, w_{ij} is the weight of

synaptic connection from neuron j to neuron i and $y_{ij}(t)$ is the amount of active neurotransmitter of neuron j, calculated according to Tsodyks-Markram equations [31]

$$\begin{aligned}
\frac{dx_{ij}}{dt} &= \frac{z_{ij}}{\tau_{rec}} - f_{ij}x_{ij}\delta(t-(t_{sp}+d_{ij})),\\
\frac{dy_{ij}}{dt} &= -\frac{y_{ij}}{\tau_1} - f_{ij}x_{ij}\delta(t-(t_{sp}+d_{ij})),\\
\frac{dz_{ij}}{dt} &= \frac{y_{ij}}{\tau_1} - \frac{z_{ij}}{\tau_{rec}},\\
\frac{df_{ij}}{dt} &= -\frac{f_{ij}}{\tau_{facil}} + U(1-f_{ij})\delta(t-(t_{sp}+d_{ij})),
\end{aligned} \tag{3}$$

where x, y, z are the fractions of synaptic resource in the recovered, active, and inactive states respectively, t_{sp} is time of spike arrival to the presynaptic terminal, d_{ij} is axonal conduction time delay taken to be proportional to the distance between ith and jth neurons. τ_1 is the decay constant of postsynaptic currents, τ_{rec} is the recovery time from synaptic depression. The variable f describes the effective use of the synaptic resources, i.e. f is increased with each presynaptic spike and returns to its baseline with a time constant τ_{facil}. The parameter U determines the change in the value of facilitation variable f when a presynaptic spike is generated. Throughout the paper we used $\tau_{rec} = 50\,\text{ms}$, $\tau_1 = 10\,\text{ms}$, $\tau_{facil} = 1000\,\text{ms}$ and $U = 0.5$.

Long-term changes in synaptic weights were modeled by classical STDP rule implemented with two local variables [8,10]. Let us consider a weight w_{ij} between two neurons: j (presynaptic) and i (postsynaptic). A presynaptic spike induces a weight decrease proportional to the value of the postsynaptic trace s_i. Similarly, a postsynaptic spike induces a weight potentiation proportional to the value of the presynaptic trace s_j:

$$\begin{aligned}
\frac{ds_i}{dt} &= -\frac{s_i}{\tau_i} + \sum_{t^i_{sp}} \delta(t-(t^i_{sp})),\\
\frac{ds_j}{dt} &= -\frac{s_j}{\tau_j} + \sum_{t^j_{sp}} \delta(t-(t^j_{sp})),\\
\frac{dw_{ij}}{dt} &= -F_-(w_{ij})s_i\delta(t-(t^j_{sp})) + F_+(w_{ij})s_j\delta(t-(t^i_{sp})).
\end{aligned} \tag{4}$$

Here s_i and s_j are the local variables denoting the postsynaptic and presynaptic traces respectively. τ_i and τ_j are their respective time constants. t^j_{sp} and t^i_{sp} are pre- and postsynaptic spike timings respectively. Weight dependence $F(w_{ij})$ was taken to obey the multiplicative update rule [9,10]:

$$\begin{aligned}
F_+(w_{ij}) &= \lambda(1-w_{ij}),\\
F_-(w_{ij}) &= \lambda\alpha w_{ij},
\end{aligned} \tag{5}$$

where λ is the learning rate and α is an asymmetry parameter. Throughout the paper we used the following values of STDP parameters: $\tau_{pre} = \tau_{post} = 20\,\text{ms}$, $\lambda = 0.001$ and $\alpha = 5$.

The network was composed of 500 neurons (400 excitatory and 100 inhibitory) randomly distributed on 2D surface. We used the following connectivity rule to define the range of the index j for each ith neuron in (2). Each ith neuron had the number of input connections taken from a Gaussian distribution with mean 15 and standard

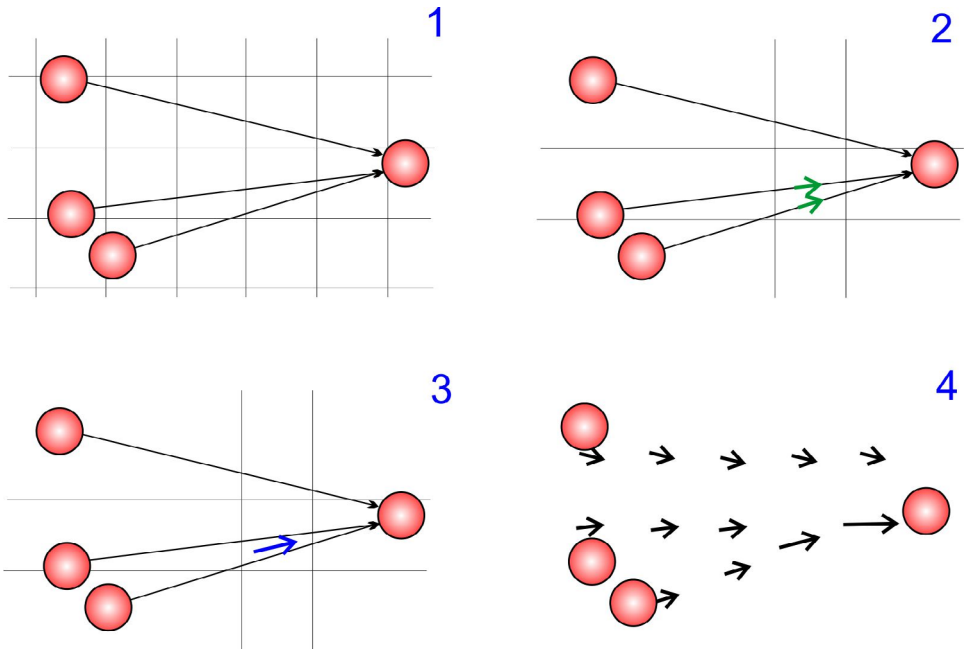

Fig. 1. Schematic representation of algorithm for calculating the vector field.

deviation 2. Then we sorted indexes of all the neurons according to the distance from those neurons to the ith neuron. To connect neurons to the ith neuron, we took indexes from this sorted array according to a Gaussian distribution with mean 0 (index of the closest neuron) and standard deviation 15. Therefore each neuron had about 15 input connections with predominance of local connections, i.e. most of the input connections are local, however some of them are distant. Signal conduction delays were proportional to the distance between neurons. The maximal value of delay between two distant network regions was 40 ms. Initial synaptic weights w_{ij} were taken from a Gaussian distribution with mean 0.5 and standard deviation 0.1. With those parameter values the network dynamics reproduced experimentally observed activity patterns of living neural networks cultured on MEA [26,32]. Particularly, the network exhibits population bursts, e.g. network-scaled synchronized events intermittent with relatively low level of asynchronous activity.

2.2 Network visualization

In order to represent network state we have developed an algorithm for visualization of synaptic weights in the form of vector field detecting average direction and strength of all the connections passing particular area. Steps of the algorithm for the construction of the vector field are shown in Fig. 1.

1. The network area was divided by a grid of square cells. In our simulations the grid contained 24×24=576 cells.
2. The network was represented as directed graph with nodes denoting the neurons and edges denoting the connections between them. All the edges crossing a particular cell of the grid were represented as vectors with direction corresponding to this edge and length proportional to the connection strength.

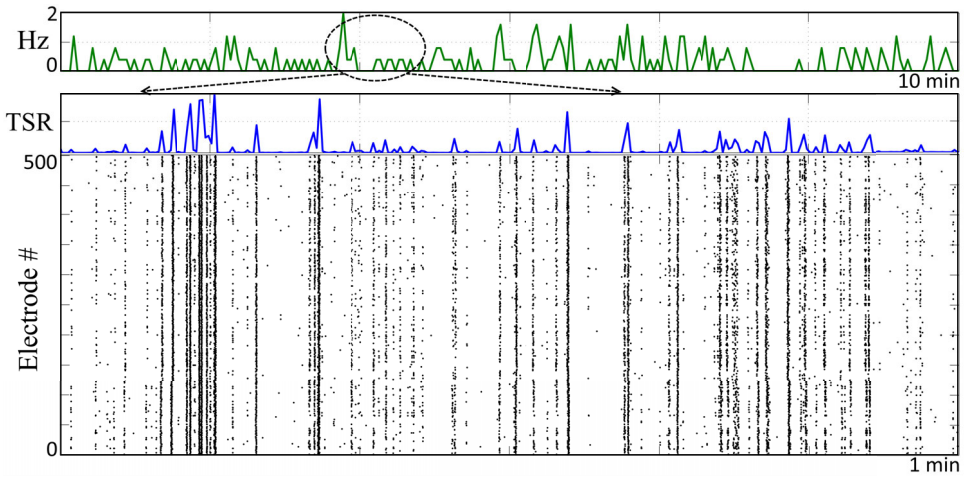

Fig. 2. Network dynamics in the autonomous mode. From top to bottom: burst frequency, TSR, raster plot.

3. For each grid cell a total vector was calculated as vector sum of all edge vectors.
4. The total vector field was plotted.

Network connectivity visualization by the vector field permits to monitor network structure in the form of static spacial weight distribution and by directions of dynamical signal transmission. In a vast majority of cases the direction of spike propagation match with direction of vector fields arrows (see supplementary material video 1 and 2).

It is remarkable, that different neurons may play different roles in population burst generation. Activation of some of them can evoke a general network response, e.g. the population burst. We classify these neurons as "hubs". The rest neurons can only contribute to population busts generation together with their spiking neighbors. To detect hubs we used the following simple procedure. The network was taken in the quiescent state with zero noise and having all synaptic resources completely recovered. Each neuron of the network was then subsequently stimulated to produce single spike. If after the stimulation, the network generated more than 50 spikes during 100 ms, this response was classified as a population burst and the neuron was assigned as a hub.

3 Results

3.1 Network dynamics in the autonomous mode

First, let us consider autonomous network dynamics. Single neurons fed by noise can be sporadically activated and spikes emitted by the neurons propagate to other neurons, which in turn can involve the whole network to generate population burst event [33]. Once initiated the population burst decays due to the short-term depression of the excitatory connections (3) and activation of the inhibitory population [31,34]. The long-term synaptic plasticity mechanism (4) causes rearrangement of synaptic weights. As a result, after several minutes of simulation time, the weight distribution becomes heterogeneous [8,9,15] and the network converges to a balanced mode characterized by irregular generation of population bursts with burst frequency varying from 0.1 to 2 Hz. Figure 2 shows an example of the network activity after the

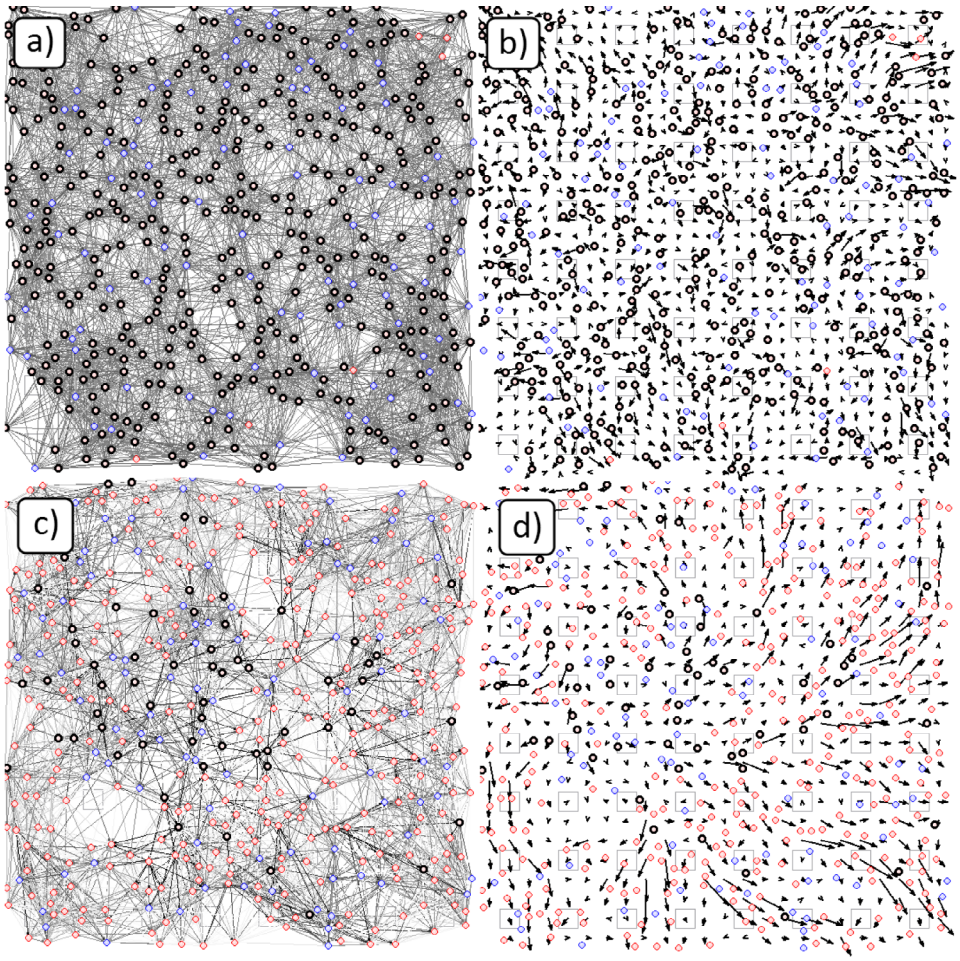

Fig. 3. Network structure before (a and b) and after (c and d) STDP-driven weight rearrangement. Neurons are shown as circles with thick black rings denoting hubs, red fills denoting excitatory neurons and blue fills denoting inhibitory neurons. a) and c) show connections visualized by lines with black saturation proportional to weight values (white color corresponds to $w_{ij} = 0$, black color corresponds to $w_{ij} = 1$). b) and d) show the vector fields.

STDP-evoked weight rearrangement. Top panel shows population burst frequency trace during 10 minutes of simulation time. A fragment of total spike rate (TSR) calculated among all the neurons in 50 ms bin is shown in the middle panel. The bottom panel shows the same fragment of raster plot of network activity where each dot represents spike generated by corresponding neuron.

To illustrate weight rearrangements during autonomous network activity we plot the network structure in the initial state (Fig. 3a and b) and after STDP-driven changes in the connection strengths (Fig. 3c and d). Note that during the simulation, initially homogeneous synaptic weights transformed to the heterogeneous distribution as illustrated in Fig. 3a and c. It is important that the vector fields (Fig. 3b and d) originated from initially random state becomes directed and acquires preferable pathways of signal transmission. Note also the decrease of the number of hubs associated with synaptic weight rearrangement.

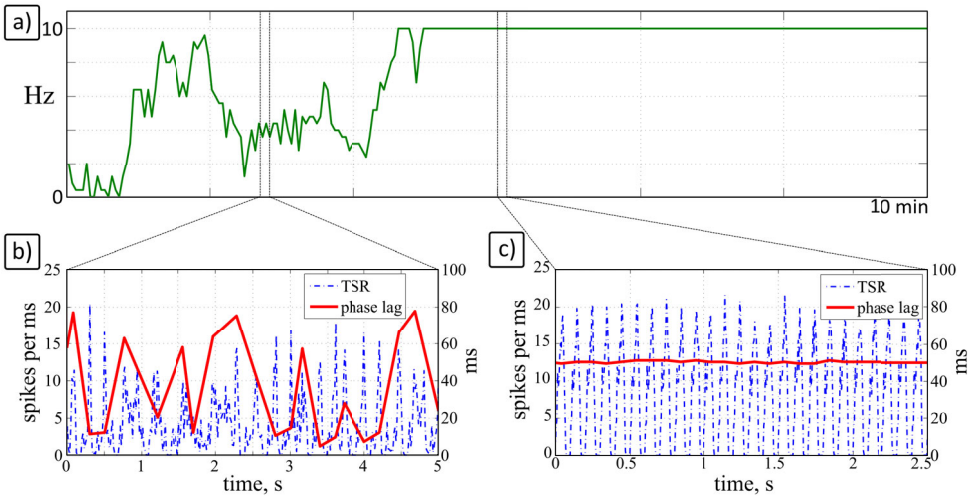

Fig. 4. Network synchronization under external periodic stimulation with input frequency of 10 Hz. a) Burst frequency trace. b) Fragment of the transient process. c) Fragment of the phase-locking mode. Blue dashed lines (colored online) show TSR traces, red solid lines (colored online) represent the phase lag.

3.2 Synchronization under external periodic signal

Let us consider now the effect of external periodic stimulation. The stimulus was introduced to the network by activation of an arbitrary chosen group containing one inhibitory and five excitatory neurons located in the same small network area. Each stimulus made all the neurons from the chosen group to fire, which in turn could produce population burst (see supplementary materials, video 3) depending also on particular group and mostly on the input frequency. For instance, under the stimulation with input frequency value taken from the range between 3 and 8 Hz the network immediately started to respond with one population burst per each stimulus and no spontaneous bursts appeared between the subsequent stimuli. This mode therefore could be classified as 1:1 frequency-locking mode or the entrainment mode [35]. For lower values of the input frequency, the network generated spontaneous bursts in addition to stimulus-evoked ones. Under stimulation with larger input frequency values, the network failed to respond to each stimulus. Interestingly, that for some input frequency values behind the range of 3–8 Hz, the entrainment mode could also be established after some transient process. Figure 4 illustrates establishing the entrainment mode under external periodic stimulation with the input frequency of 10 Hz. At the beginning of simulation, population bursts occurred with frequency lower than the frequency of the input stimulation (Fig. 4a) and their amplitudes varied significantly (Fig. 4b, blue dashed trace, colored online). However after about 4.5 minutes of simulation time the transient process led to the stable frequency-locking mode. In this mode the burst frequency became equivalent to the input frequency (Fig. 4a) and the burst amplitude became stable (Fig. 4c, blue dashed trace, colored online). To classify the observed synchronization mode we calculated phase of response defined in [35,36] as difference between timings of the maximal value of TSR achieved during each population burst and the timings of corresponding stimuli (shown in Fig. 4b and c, solid red trace, colored online). The phase exhibiting high variability during the transient period (Fig. 4b) was stabilized after establishing the frequency-locking mode (Fig. 4c). The observed mode of evoked synchronization was

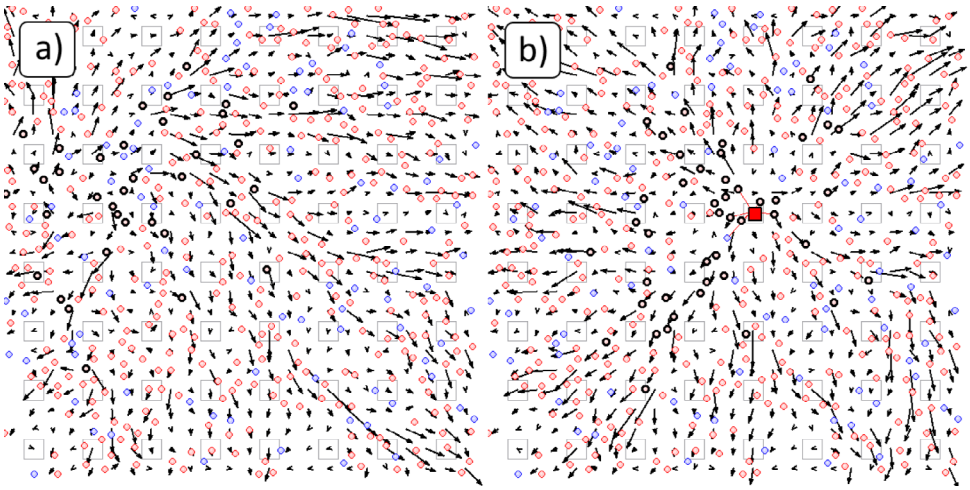

Fig. 5. Visualization of network structure as a vector fields before (a) and after (b) periodic stimulation applied with frequency of 10 Hz.

therefore the phase-locking mode. Typically, in our simulations the phase lag in the phase-locking mode was stable and consisted about 50 ms.

We further investigate the mechanisms underlying this transient process leading to establishment of the phase-locking mode. Figure 5 shows the vector fields of the simulated network before (a) and after (b) periodic stimulation applied with frequency of 10 Hz. The source of external stimuli marked by red square (Fig. 5b, colored online) indicates the location of the stimulated group. Difference between the two vector fields indicated that the STDP-driven synaptic updates led structural changes occurred at the network scale. It appeared that the balanced weight distribution established during autonomous dynamics, was rearranged after applying periodic stimulation. This rearrangement reflected changes in signal transmission pathways gained predominantly divergent structure with prevalent directions of signal transmission from the stimulation site towards the neighboring neurons, whereas the other directions of signal transmission disappeared or became less expressed. The new gained structure could facilitate population burst generation in response to the external stimuli applied locally at that particular stimulation site, which in turn led to the phase-entrainment dynamics. It is noteworthy that different locations of the chosen stimulated group led to similar results of redirecting the vector field. The role of STDP-driven structural changes can also be seen comparing hub distributions before and after the stimulation.

To reveal the role of STDP-driven weight rearrangements in establishing the synchronized mode, we simulated the network with and without STDP update rule, under external periodic stimulations with different frequencies. During these simulations we monitored population burst frequency normalized on the input frequency and the phase lag observed in the synchronized state. The results are shown in Fig. 6, where the blue lines (colored online) with square markers represent simulations without the STDP weight update rule, and the red lines (colored online) with circle markers represent simulations in the presence of STDP. Without STDP the network could be synchronized by the external stimuli with input frequencies taken only between 5 and 8 Hz (Fig. 6a). Similarly, the phase lag in the synchronized state was stable and had low variability among responses to different stimuli (Fig. 6b) only for input frequencies taken from this range. In contrast, when the STDP update rule was activated the synchronized state could be achieved for much wider range of input

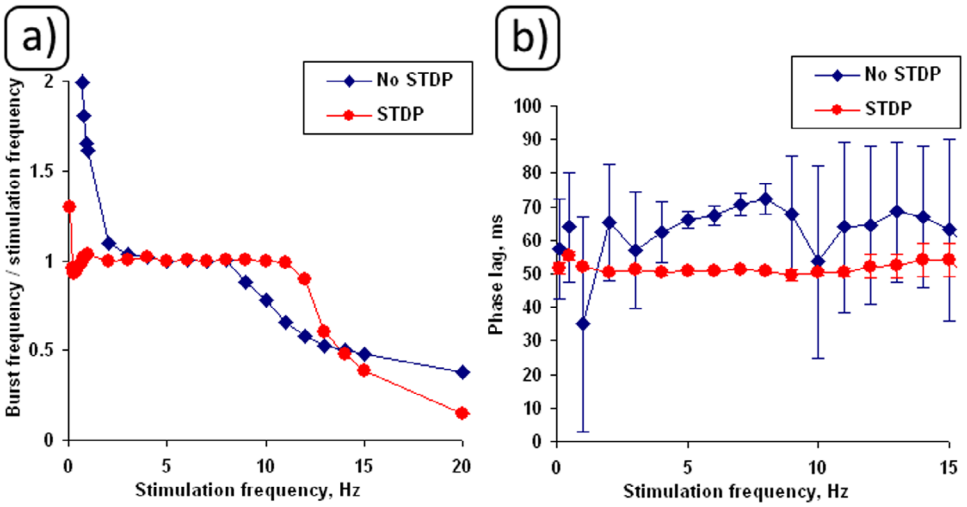

Fig. 6. Normalized population burst frequency (a) and phase lag in the synchronized state (b) depending on the input frequency. Blue lines with square markers represent simulations without STDP weight update rule. Red lines with circle markers represent simulations in the presence of STDP.

frequencies. It is illustrated in the graph depicting the normalized burst frequency (Fig. 6a) and in the graph of the phase lag (Fig. 6b).

4 Discussion

We investigated the effect of network-level synchronization by local periodic stimulation and analyzed the role of the synaptic dynamics in this process. The synchronization phenomenon is believed to play an important role in the organizing functional neural ensembles in the brain. Synchronous oscillations and propagating waves involve global activation of large-scale brain networks clocking formation of memory traces, learning and other cognitive processes. On the other side, local changes in the efficacy of synaptic transmission governed by STDP and other Hebbian-like plasticity rules can be also considered as biophysical substrate of information processing in the brain. We believe that the effect of STDP-driven network synchronization found in our model can be considered as a link between these two spacial scales of brain functioning. It can also act as a binding mechanism between the network-level memory formation and the local level of synaptic plasticity.

Our model predicted that the effect of synaptic plasticity can significantly enhance frequency band of the synchronization. Interestingly, that bi-directional interaction between STDP and synchronization may impact on signalling at network scale. Indeed, the high level of network synchrony, from the one hand, may lead to occurrence of many precise coincidences of spike-timings causing STDP-driven local changes of synaptic weights. And on the other hand, as we have demonstrated, STDP-driven changes of synaptic weights can increase network-level synchrony.

The developed vector field approach permitted to reveal the role of STDP-driven structural changes in the effect of establishing the phase-entrainment mode with stable phase lag. We have found that locally applied stimulation led to rearrangement of the synaptic weights and to formation of the “trodden” pathways diverging from the stimulus site towards the rest of the network. Thus the rearranged structure facilitates

generation of similar responses on each subsequent stimulus applied to the same site. Such stimulus-evoked activity can be compared to a surface wave propagating from the perturbation spot (see supplementary materials, video 3 and video 4). Similar responses propagating through the same synaptic pathways cause stable frequency and phase lag.

To monitor changes in the structure and reveal their impact on the network dynamics we detected the activity hubs. Considering hub distributions we also conclude that the hubs tend to form clusters during either the autonomous or evoked dynamics (see Fig. 5). Such clustering can form an activity focus (or several foci) of the network determining the initial site of population burst generation similar to burst leader neurons [37,38]. Their rearrangement by an external stimulation can significantly alter the network dynamics.

Several interesting questions can be formulated based on our results. (i) How long can the stimulus-driven rearrangements remain after the stimulation is switched off? This can be considered as "forgetting" the learned stimulation pattern. (ii) Can the stimulus driven synchronization be achieved faster that in our simulations, if we use different parameter values? (iii) Does short-term plasticity and signal conduction delays play a critical role in the stimulus driven synaptic weights rearrangements and their preserving after switching off the stimulation? They have to be considered in future investigations.

Finally, our results may also predict new experimental findings on stimulus-evoked synchronization of the cultured networks. Considering recordings made under control conditions with those made in the presence of chemicals blocking STDP-evoked changes, one can expect that in the latter case the range of stimulation frequency inducing network-level synchronization should dramatically decrease or even disappear in comparison to the control experiments.

This work was supported by the Russian Science Foundation project 14-19-01381.

References

1. G. Buzsaki, *Rhythms of the Brain* (Oxford University Press, 2009)
2. X.-J. Wang, Physiol. Rev. **90**, 1195 (2010)
3. E. Salinas, T.J. Sejnowski, Nature Rev. Neurosci. **2**, 539 (2001)
4. J.L. Rossello, V. Canals, A. Oliver, A. Morro, Int. J. Neural Syst. **24**, 1430003 (2014)
5. W.W. Lytton, Nat. Rev. Neurosc. **9**(8), 62637 (2008)
6. H. Markram, J. Lubke, M. Frotscher, B. Sakmann, Science **275**, 213 (1997)
7. G. Bi, M. Poo, J. Neurosci. **18**, 10464 (1998)
8. S. Song, K.D. Miller, L.F. Abbott, Nat. Neurosci. **3**, 919 (2000)
9. R. Gutig, R. Aharonov, S. Rotter, H. Sompolinsky, J. Neurosci. **23**, 3697 (2003)
10. A. Morrison, M. Diesmann, W. Gerstner, Biol. Cybern. **98**, 459 (2008)
11. M. Gilson, A. Burkitt, J.L. van Hemmen, Front. Comput. Neurosci. **4**, 23 (2010)
12. C. Clopath, L. Buesing, E. Vasilaki, W. Gerstner, Nature Neurosci. **13**, 344 (2010)
13. V. Kazantsev, I. Tyukin, PloS One **7**, e30411 (2012)
14. M. Graupner, N. Brunel, PLoS Comput. Biol. **3**, e221 (2007)
15. E.M. Izhikevich, J.A. Gally, G.M. Edelman, Cereb. Cortex **14**, 933 (2004)
16. E.M. Izhikevich, Neural Comput. **18**, 245 (2006)
17. T. Nowotny, V.P. Zhigulin, A.I. Selverston, H.D.I. Abarbanel, M.I. Rabinovich, J. Neurosci. **23**, 9776 (2003)
18. Y. Ruan, G. Zhao, Neural Plast. **2009**, 704075 (2009)
19. J.-P. Pfister, P.A. Tass, Front. Comput. Neurosci. **4**, 22 (2010)
20. E.V. Lubenov, A.G. Siapas, Neuron, **58**(1), 11831 (2008)
21. D.A. Wagenaar, J. Pine, S.M. Potter, BMC Neurosci. **7**, 11 (2006)

22. M. Chiappalone, M. Bove, A. Vato, M. Tedesco, S. Martinoia, Brain Res. **1093**, 41 (2006)
23. L.L. Bologna, T. Nieus, M. Tedesco, M. Chiappalone, F. Benfenati, S. Martinoia, Neuroscience **165**, 692 (2010)
24. L. Berdondini, P. Massobrio, M. Chiappalone, M. Tedesco, K. Imfeld, A. Maccione, M. Gandolfo, M. Koudelka-Hep, S. Martinoia, J. Neurosci. Meth. **177**, 386 (2009)
25. A. Maccione, M. Gandolfo, P. Massobrio, A. Novellino, S. Martinoia, M. Chiappalone, J. Neurosci. Meth. **177**, 241 (2009)
26. A. Pimashkin, I. Kastalskiy, A. Simonov, E. Koryagina, I. Mukhina, V. Kazantsev, Front. Comput. Neurosci. **5**, 46 (2011)
27. G. Shahaf, S. Marom, J. Neurosci. **21**, 8782 (2001)
28. J. le Feber, J. Stegenga, W.L. Rutten, PLoS One **5**, e8871 (2010)
29. A. Pimashkin, A. Gladkov, I. Mukhina, V. Kazantsev, Front. Neural Circuits **7**, 87 (2013)
30. E.M. Izhikevich, IEEE Trans. Neu. Net. **14**, 1569 (2003)
31. M. Tsodyks, A. Uziel, H. Markram, J. Neurosci. **20**, 825 (2000)
32. D.A. Wagenaar, R. Madhavan, J. Pine, S.M. Potter, J. Neurosci. **25**, 680 (2005)
33. A.Y. Simonov, V.B. Kazantsev, JETP Letters **93**, 470 (2011)
34. T.A. Gritsun, J. le Feber, J. Stegenga, W.L.C. Rutten, Biol. Cybern. **102**, 293 (2010)
35. E.M. Izhikevich, *Dynamical Systems in Neuroscience* (The MIT Press, Cambridge, Massachusetts, 2007)
36. A. Pikovsky, M. Rosenblum, J. Kurths, *Synchronization: a universal concept in nonlinear sciences* (Cambridge University Press, New York, 2003)
37. J.-P. Eckmann, S. Jacobi, S. Marom, E. Moses, C. Zbinden, New J. Phys. **10**, 015011 (2008)
38. V. Pasquale, S. Martinoia, M. Chiappalone, BMC Neurosci. **14**, 64 (2013)